NASA TECHNICAL NOTE

NASA TN D-2833



# INVESTIGATION OF EFFECTS OF RAMP SPAN AND DEFLECTION ANGLE ON LAMINAR BOUNDARY-LAYER SEPARATION AT MACH 10.03

*by Lawrence E. Putnam*

*Langley Research Center*

*Langley Station, Hampton, Va.*

NATIONAL AERONAUTICS AND SPACE ADMINISTRATION • WASHINGTON, D. C. • MAY 1965

NASA TN D-2833

# INVESTIGATION OF EFFECTS OF RAMP SPAN AND DEFLECTION ANGLE ON LAMINAR BOUNDARY-LAYER SEPARATION AT MACH 10.03

By Lawrence E. Putnam

Langley Research Center
Langley Station, Hampton, Va.

NATIONAL AERONAUTICS AND SPACE ADMINISTRATION

For sale by the Clearinghouse for Federal Scientific and Technical Information
Springfield, Virginia 22151 – Price $2.00

# INVESTIGATION OF EFFECTS OF RAMP SPAN AND DEFLECTION ANGLE ON LAMINAR BOUNDARY-LAYER SEPARATION AT MACH 10.03[1]

By Lawrence E. Putnam
Langley Research Center

## SUMMARY



An investigation has been made in the Langley 15-inch hypersonic flow apparatus to establish the extent and magnitude of the separation-induced pressure distribution on flat surfaces ahead of small-span ramps and to evaluate the usefulness of two-dimensional separation theory for correlating and predicting the characteristics of laminar separation in three-dimensional flow. Pressure distributions were obtained on a flat plate with an aft-mounted ramp at a Mach number of 10.03 and Reynolds numbers per inch of approximately $1.27 \times 10^5$ and $1.53 \times 10^5$. The ramp deflection angle was varied from $0^\circ$ to $40^\circ$ and the ratio of the ramp span to the ramp chord (the ramp aspect ratio) was varied from 2 to 4 by varying the ramp span.

The experimental results indicate that increasing the deflection angle of a finite-span ramp from $10^\circ$ to $40^\circ$ results in increases in the length of the separated region along the model center line and in the magnitude of the pressures in the separated region. Decreasing the ramp aspect ratio from 4 to 2 at a given deflection angle results in decreases in the magnitude of the pressures in the separated region. The separation length along the model center line decreases almost linearly with decreasing aspect ratio for constant ramp angles; however, the separation length is more strongly influenced by aspect ratio as the ramp deflection angle is increased. Data for the ramps of aspect ratio 2 and oil-flow observations indicate that the separation-induced pressure rise extends a considerable distance outboard of the lateral edge of the finite-span ramps. Methods suggested by two-dimensional separation theory generally result in a good correlation of the plateau-pressure data obtained on the center line of the model with Reynolds number and Mach number. Author

---

[1]The basic information presented herein was a part of a thesis entitled "An Experimental Investigation of the Effects of Ramp Aspect Ratio and Deflection Angle on Laminar Boundary-Layer Separation in Hypersonic Flow" which was offered in partial fulfillment of the requirements for the degree of Master of Aerospace Engineering, University of Virginia, Charlottesville, Virginia, August 1964.

## INTRODUCTION

Shock-induced boundary-layer separation on aerodynamic surfaces is a phenomenon of common occurrence in supersonic and hypersonic flows. Large changes in the stability and trim of a vehicle in hypersonic flight may occur as a result of shifts in the center of pressure and changes in the magnitude of the pressure level on control surfaces and adjacent aerodynamic surfaces due to the occurrence of flow separation. The performance of inlets on hypersonic aircraft may also be seriously affected by boundary-layer separation ahead of inlet compression surfaces. The adequate prediction of such changes in the aerodynamic properties of hypersonic aircraft requires a detailed knowledge of both the characteristics of and the parameters governing flow separation at hypersonic speeds. The study of hypersonic boundary-layer separation phenomena is important as a result of the great interest presently exhibited in the development of high-speed vehicles.

The effects of flow separation on the surface pressure distribution are greatly influenced by the type of boundary-layer flow approaching the separation point; that is, whether the boundary layer is laminar, transitional, or turbulent. The experimental data of reference 1 show a marked increase in the magnitude of the transition Reynolds number (based on downstream distance of the transition point) with increasing Mach number. These results indicate that a knowledge of laminar boundary-layer separation phenomena becomes increasingly important for hypersonic speeds.

Many experimental and theoretical investigations of laminar boundary-layer separation at supersonic speeds have been made in the past. (See, for example, refs. 2 to 18.) References 17 and 18 contain comprehensive reviews of the available experimental and theoretical results from investigations of supersonic boundary-layer separation. For hypersonic flows, however, relatively little experimental or theoretical information on boundary-layer separation is available. (See refs. 19 to 27.) Most of the experimental and theoretical investigations of shock-induced separation for both supersonic and hypersonic flows to date have been concerned principally with two-dimensional flow regimes. In most problems of practical importance, however, three-dimensional flow is present, and lateral flow into or out of separation zones may appreciably alter the shape and extent of the separated region, with resultant alteration of the induced pressure field on the surface. The shape of a separation zone in two-dimensional flow is dependent on the volume of fluid trapped within the separated region. The low-momentum fluid in the high-pressure separation zone responds readily, however, to lateral pressure gradients which may exist; large changes in the separation pressure distribution can thereby result because of the partial collapse of the separated region in three-dimensional flow. This problem of three-dimensional venting or "bleed out" of the low-energy air in the separated region from the spanwise extremities of ramps of finite span may have large effects on the aerodynamic control effectiveness and the performance of some types of air inlets. The magnitudes of these effects on the pressure distribution in the separated region depend primarily on the span of the ramp if reattachment of the boundary layer occurs on the ramp surface. That is, for a given ramp span, increasing the ramp chord

beyond that required for reattachment of the separated boundary layer should not significantly affect the pressure distribution in the separated region.

The purpose of the present investigation is to establish the extent and magnitude of the separation-induced pressure field on flat surfaces ahead of small-span ramps and to evaluate the usefulness of theory for two-dimensional flow for correlating and predicting the separation-flow parameters in cases where three-dimensional flow effects are significant (i.e., for ramps of small span). In particular, the investigation was undertaken to determine experimentally the effects of ramp span and ramp deflection angle on the characteristics of separated laminar flow at hypersonic speeds and to compare the experimental results with the predictions of two-dimensional boundary-layer separation theory.

The investigation was made in the Langley 15-inch hypersonic flow apparatus at a Mach number of 10.03 and free-stream Reynolds numbers per inch of approximately $1.27 \times 10^5$ and $1.53 \times 10^5$. Pressure distributions were obtained on a flat plate with an aft-mounted ramp. The deflection angle of the ramp was varied from $0^\circ$ to $40^\circ$ in increments of $10^\circ$, and the ratio of the ramp span to the ramp chord (the ramp aspect ratio) was varied from 2 to 4 by varying the ramp span.

## SYMBOLS

| | |
|---|---|
| $A$ | ramp aspect ratio, $b/c$ |
| $b$ | ramp span |
| $C_A$ | axial-force coefficient |
| $C_m$ | pitching-moment coefficient |
| $C_N$ | normal-force coefficient |
| $C_p$ | pressure-rise coefficient, $\frac{2}{\gamma M_o^2}\left(\frac{p}{p_o} - 1\right)$ |
| $c$ | ramp chord |
| $c_f$ | local skin-friction coefficient |
| $K$ | constant of proportionality in equation (2) |
| $l_i$ | characteristic streamwise length over which interaction takes place |
| $l_{sep}$ | separation length, distance from separation point to ramp leading edge along x-axis |
| $M$ | Mach number |

$p$ pressure

$p_t'$ pitot pressure

$q$ dynamic pressure, $\frac{\gamma p M^2}{2}$

$R$ local Reynolds number based on free-stream conditions, $\frac{\rho_\infty V_\infty x}{\mu_\infty}$

$R_{x,o}$ Reynolds number at beginning of pressure interaction, $\frac{\rho_o V_o x_o}{\mu_o}$

$r$ leading-edge radius of plate

$T$ temperature

$V$ velocity

$x$ longitudinal coordinate (see fig. 2)

$y$ lateral coordinate (see fig. 2)

$z$ vertical coordinate (see fig. 2)

$\alpha$ angle of attack

$\beta = \sqrt{M^2 - 1}$

$\gamma$ ratio of specific heats

$\Delta$ canard-surface deflection angle

$\delta$ boundary-layer thickness

$\delta^*$ boundary-layer displacement thickness

$\epsilon$ $\frac{d\delta^*}{dx}$ in separation region

$\theta$ ramp deflection angle

$\mu$ coefficient of viscosity

$\xi$ interaction pressure ratio, $\frac{p_o}{p_\infty}$

$\rho$ mass density of air

Subscripts:

| | |
|---|---|
| aw | adiabatic wall |
| e | condition at edge of boundary layer |
| f | final condition on ramp |
| o | condition at beginning of interaction |
| p | condition in region of pressure plateau |
| s | condition at separation |
| t | stagnation condition |
| w | condition on surface (wall) of model |
| $\infty$ | free-stream condition |

## REVIEW OF BOUNDARY-LAYER SEPARATION THEORY

Although numerous theoretical methods are available for predicting the onset of boundary-layer separation and the characteristics of two-dimensional separated flow, none of the available theoretical solutions are in good quantitative agreement with experimental data. Boundary-layer separation information useful for design purposes has been based primarily on experimental data and semiempirical methods.

The pressure distribution on a flat plate with a separated two-dimensional laminar boundary layer has a characteristic plateau where the pressure remains almost constant over most of the separated region. This constant-pressure region is illustrated in figure 1, which shows a typical pressure distribution resulting from a separated laminar boundary layer. This figure also shows a sketch of the physical flow field and defines the quantities which are used in the analysis of boundary-layer separation.

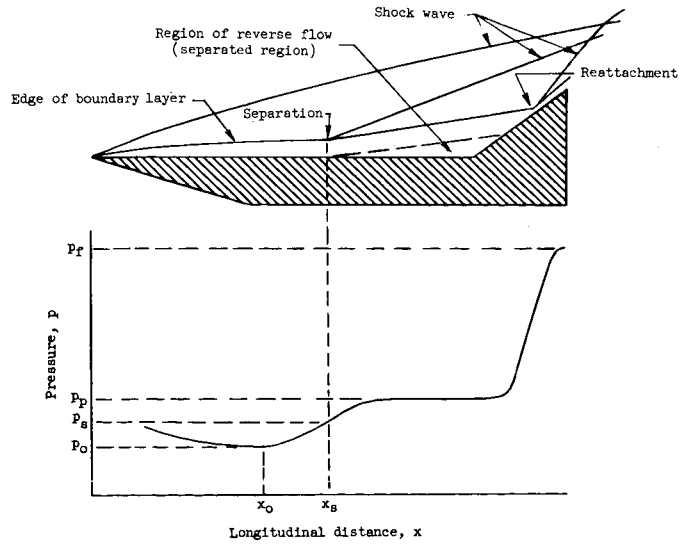


Figure 1.- Sketch showing characteristics of a separated laminar boundary layer.

The analyses of references 2 and 5 have illustrated that when an appreciable length of separated

flow exists in two-dimensional flow, the conditions at the separation point and in the separated region are essentially independent of the geometric shapes inducing the separation, and therefore the separation phenomena involved are essentially similar. That is, the significant flow parameters are functions only of Mach number, Reynolds number, and surface wall temperature. Thus, the analysis of shock-induced boundary-layer separation may be broken into two parts: (1) the determination of similar separation properties such as the separation and plateau pressures; and (2) the determination of the length of the separated region.

The significant parameters necessary to describe the characteristics of a separated boundary layer are the pressure rise from the start of the separation interaction $x_o$ to the separation point $x_s$ and the pressure rise from $x_o$ to the pressure plateau. From consideration of order-of-magnitude arguments, Chapman and his coworkers (ref. 2) concluded, from the momentum equation for steady two-dimensional flow in a viscous boundary layer and the equation for the inviscid supersonic flow external to the boundary layer, that the pressures anywhere in the separated region are functions of the Mach number and the skin-friction coefficient at $x_o$; namely,

$$\frac{p - p_o}{q_o} \propto \left( \frac{c_{f,o}}{\sqrt{M_o^2 - 1}} \right)^{1/2} \tag{1}$$

Inasmuch as the laminar skin-friction coefficient is inversely proportional to the square root of the Reynolds number, equation (1) can be written as

$$\frac{p - p_o}{q_o} = \frac{K}{\beta_o^{1/2} R_{x,o}^{1/4}} \tag{2}$$

The best fit to the experimental data of reference 2 indicates that the constant $K$ in equation (2) has the value 1.82 for the plateau pressure-rise coefficient $C_{p,p}$, and 0.93 for the separation pressure-rise coefficient $C_{p,s}$.

Relationships for the separation and plateau pressure-rise coefficients derived in references 3 and 4 are similar to equation (2) but have different values for the constant of proportionality. A comparison of these constants of proportionality as determined in references 2, 3, and 4 is shown in the following table:

| Reference | Author | $M_\infty$ range | $K_s$ | $K_p$ |
|---|---|---|---|---|
| 2 | Chapman, Kuehn, and Larson | $1 < M_\infty < 3.6$ | 0.93 | 1.82 |
| 3 | Hakkinen, Greber, Trilling, and Abarbanel | $M_\infty = 2$ | 1.15 | 1.90 |
| 4 | Gadd | $M_\infty > 1$ | 1.13 | ---- |

In reference 17 equation (2) was rewritten for the variation of pressure in the region of a separated laminar boundary layer in terms of certain universal empirical functions, with the result that

$$\left(\frac{p - p_o}{q_o}\right) R_{x,o}^{1/4} = f\left(\frac{x - x_o}{l_i}\right) g\left(M_o, \frac{T_{w,o}}{T_{e,o}}\right) \tag{3}$$

where

$$g\left(M_o, \frac{T_{w,o}}{T_{e,o}}\right) = \sqrt{\frac{2c_{f,o} R_{x,o}^{1/2}}{\beta_o}} \tag{4}$$

The values of the function f were determined experimentally by using one set of pressure measurements for a free interaction in laminar flow ($M_o = 2$ and $R_{x,o} = 6.75 \times 10^4$) taken from reference 2. In reference 17, it was found that at separation

$$f\left(\frac{x - x_o}{l_i}\right) = f\left(\frac{x_s - x_o}{l_i}\right) = 0.81$$

and in the region of the constant-pressure plateau

$$f\left(\frac{x - x_o}{l_i}\right) = f(1) = 1.47$$

This method considers the effect of wall temperature on boundary-layer separation.

An analysis of the separated region in reference 3 showed that the separation length is almost proportional to the pressure rise in excess of that required to induce incipient separation and that the separation length varies only weakly with Reynolds number; thus,

$$l_{sep} \propto \frac{1}{R_{x,o}^{1/8}} \left(C_{p,f} - 2C_{p,s}\right) = \frac{\left(C_{p,f} - 1.21C_{p,p}\right)}{R_{x,o}^{1/8}} \tag{5}$$

A qualitative analysis of the characteristics of laminar boundary-layer separation was made in reference 17 and indicated that

$$\frac{l_{sep}}{\delta_o} = f\left(\frac{p_f - p_p}{p_o}, \frac{1}{\epsilon}\right) \tag{6}$$

(This equation has been rewritten in the notation of the present paper. It should be noted that $l_{sep}$ as defined herein is not the same in reference 17. However, a relationship between $l_{sep}$ in the present paper and the length of separation in reference 17 is given in reference 17.) A correlation of the data of reference 3 obtained at a Mach number of 2 with separation induced by an incident shock wave was used to determine the function $f\left(\frac{p_f - p_p}{p_o}, \frac{1}{\epsilon}\right)$. However, the validity of the results of reference 17 for other Mach numbers and for other means of inducing separation has not been substantiated.

In most problems of practical importance, a separated laminar boundary layer is composed of three-dimensional rather than two-dimensional flow. Such three-dimensional effects as the venting of the separation region in front of a ramp of finite span make the theoretical analysis of three-dimensional-flow separation difficult. Some insight into the three-dimensional separation phenomenon can be gained, however, by using two-dimensional methods of analysis. Therefore, the three-dimensional results of the present investigation are compared with the predictions of two-dimensional theoretical and semiempirical methods, and the primary differences between the two-dimensional predictions and the three-dimensional experimental results are indicated.

## DESCRIPTION OF APPARATUS

### Tunnel

The investigation was conducted in the Langley 15-inch hypersonic flow apparatus. This facility is a hypersonic blowdown tunnel which operates at a Mach number of 10.03, stagnation pressures up to 1500 psia, and stagnation temperatures up to 1500° F. Details of the tunnel and its operational characteristics can be found in reference 27.

### Model

The basic model consisted of a flat plate having a sharp leading edge with a radius of less than 0.001 inch. A drawing of the model is shown in figure 2 and a photograph of the model mounted in the tunnel is shown in figure 3. Provisions were made for locating ramps of various deflection angles and spans at the rearward end of the basic flat-plate model. Three ramps were tested; all had chords of 1.25 inches and spans of 5.00 inches (A = 4), 3.75 inches (A = 3), and 2.50 inches (A = 2). Ramps of each aspect ratio were constructed with deflection angles of 10°, 20°, 30°, and 40°.

The flat plate had 21 static-pressure orifices located in three parallel, streamwise rows. (See fig. 2.) Nine pressure orifices were located on each of the ramps of aspect ratio 3 and 4, and six pressure orifices were located on

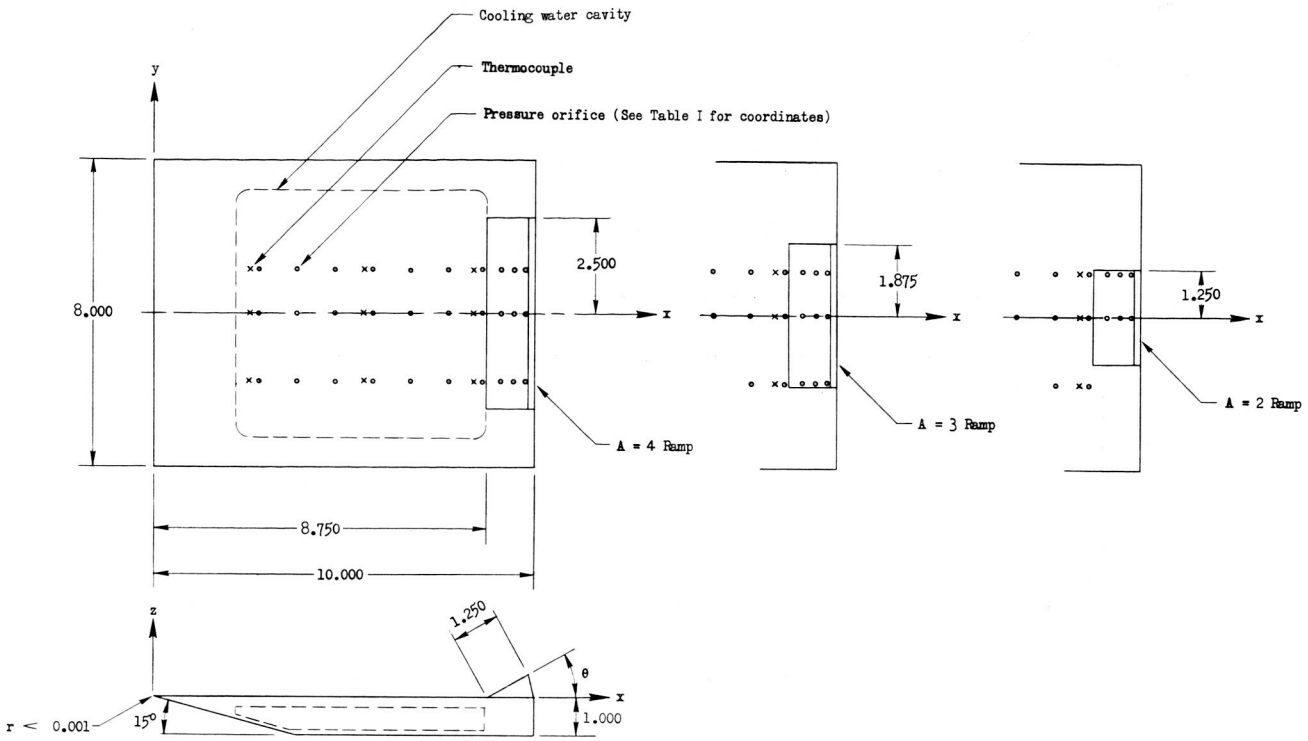


Figure 2.- Drawing of model. All dimensions are in inches unless otherwise noted.

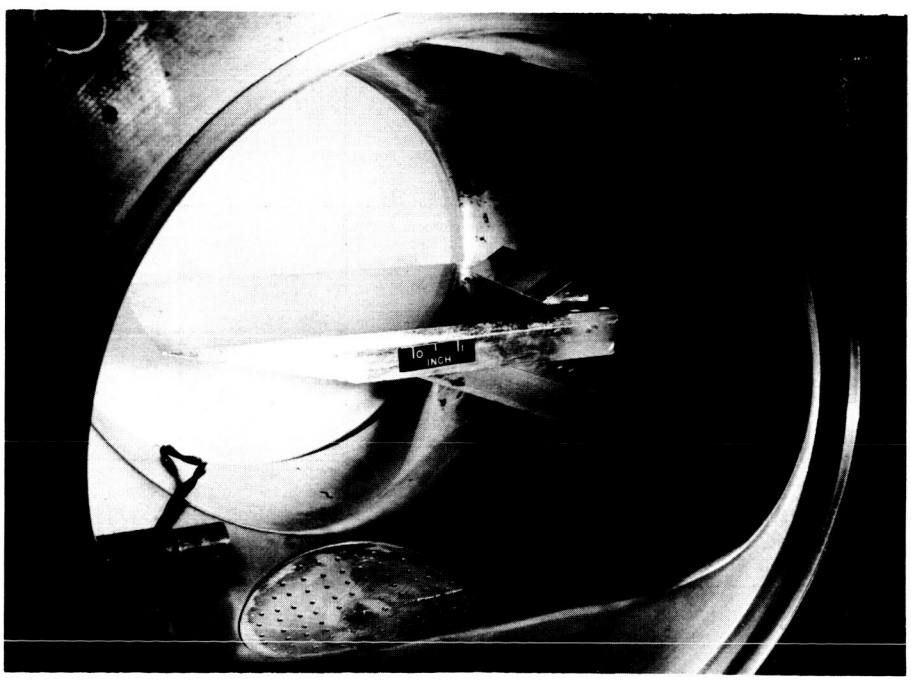


L-64-509

Figure 3.- Photograph of flat-plate model with a ramp of A = 4 deflected 30° in Langley 15-inch hypersonic flow apparatus.

the ramps of aspect ratio 2. Table I gives the coordinates of the orifice locations on the flat plate and the ramps. All orifices had a diameter of 0.060 inch.

TABLE I.- LOCATION OF PRESSURE ORIFICES ON MODEL

(a) Coordinates of orifices on flat plate

| x, in. | y, in. | | |
|---|---|---|---|
| 2.750<br>3.750<br>4.750<br>5.750<br>6.750<br>7.750<br>8.656 | 0 | 1.150 | -1.775 |

(b) Coordinates of orifices on ramps

| θ, deg | x, in. | y, in.[a] | | |
|---|---|---|---|---|
| 0 | 9.133<br>9.516<br>9.900 | 0 | 1.150 | -1.775 |
| 10 | 9.127<br>9.504<br>9.883 | 0 | 1.150 | -1.775 |
| 20 | 9.110<br>9.470<br>9.831 | 0 | 1.150 | -1.775 |
| 30 | 9.082<br>9.413<br>9.746 | 0 | 1.150 | -1.775 |
| 40 | 9.043<br>9.337<br>9.631 | 0 | 1.150 | -1.775 |

[a]The ramps of aspect ratio 2 had no orifices at $y = -1.775$.

Nine thermocouples were embedded in the surface of the flat plate to measure the wall temperature; they were placed in three parallel, streamwise rows containing three thermocouples each. The thermocouples were located at $x = 2.500$, $5.500$, and $8.405$ inches from the nose, and $y = 0$, $1.150$, and $-1.775$ inches from the center line.

The model was constructed with a hollow interior to allow water cooling during tests. The size of this cavity and the water-cooled area of the flat plate are shown in figure 2.

## Instrumentation

The static pressures of the 21 orifices on the flat plate were measured with electrical hot-wire type pressure gages having a pressure range from 0 to 20 millimeters of mercury. Pressures of the orifices on the ramps were measured with electrical strain-gage type pressure gages having a pressure range from 0 to 2 psia. The stagnation pressure was measured with an electrical pressure transducer which has a capability of measuring pressures from 0 to 2000 psig. The outputs from the pressure gages were recorded with self-balancing potentiometers having pen-type strip charts.

Model surface temperatures were measured with chromel-alumel thermocouples embedded in the model surface. The stagnation temperature of the free-stream flow was obtained with a chromel-alumel thermocouple located in the settling chamber of the tunnel. The outputs from the thermocouples were continuously recorded on the strip charts.

A reflecting-mirror schlieren system having a horizontal knife edge was used to obtain photographs of the boundary-layer growth along the surface of the model and the shock and expansion waves about the model.

## TESTS

The experiments were conducted at a free-stream Mach number of 10.03, at stagnation pressures of approximately 816 psia and 1020 psia, and at corresponding stagnation temperatures of about $1098^{\circ}$ F and $1141^{\circ}$ F, respectively. A discussion of the validity of using these stagnation temperatures, which are below the theoretical temperature required to prevent liquefaction of the air during the expansion in the tunnel, is given in the appendix. The stagnation pressures and temperatures used correspond to free-stream Reynolds numbers of approximately $1.27 \times 10^5$ and $1.53 \times 10^5$ per inch. The flat plate was maintained at an angle of attack of approximately $0^{\circ}$ and the leading-edge radius was less than 0.001 inch throughout the investigation. Tests were made with ramp deflection angles of $0^{\circ}$, $10^{\circ}$, $20^{\circ}$, $30^{\circ}$, and $40^{\circ}$, and ramp aspect ratios of 2, 3, and 4. Because the running time of the tunnel (approximately 2 minutes) was insufficient to enable the basic flat-plate surface to reach equilibrium temperature conditions (adiabatic wall temperature), the model was water cooled during each test in order to maintain an approximately constant

wall temperature at any given location on the model surface while the pressure data were being recorded. Circulating water through the model allowed approximately the same wall temperature to be maintained also at a given location on the model surface for all test runs during the investigation. Figure 4 shows the range of wall temperatures obtained on the plate during the investigation.

Surface flow patterns were obtained by use of the oil-flow technique; that is, a mixture of lubricating oil and lampblack was applied to the model surface in a dot pattern, and the model was then subjected to the air stream. Photographs of the resulting flow patterns on the various model configurations were obtained during the test runs.

## ACCURACY OF DATA

The estimated accuracies of the static-pressure data measured with the hot-wire type transducers on the flat plate and the strain-gage type transducers on the ramps are ±0.004 psia and ±0.02 psia, respectively. The stagnation-pressure measurements are estimated to have an accuracy of ±10 psia. These estimates of the accuracies of the pressure measurements are based on the linearity, hysteresis, and repeatability of the calibrations for the pressure transducers.

The wall-temperature measurements are estimated to have an accuracy of ±1° F, and the stagnation-temperature measurements have an estimated accuracy of ±4° F. The temperature accuracies are based on the accuracy of reading the strip charts and the accuracy of determining the reference temperature.

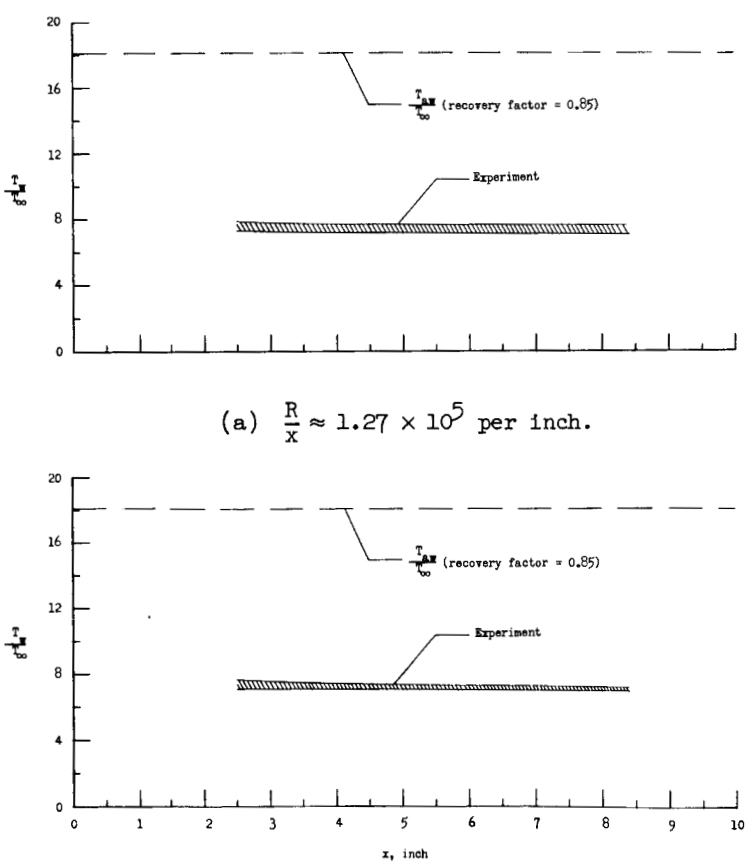


(a) $\frac{R}{x} \approx 1.27 \times 10^5$ per inch.

(b) $\frac{R}{x} \approx 1.53 \times 10^5$ per inch.

Figure 4.- Variation of wall temperature on flat plate.

## RESULTS AND DISCUSSION

As was mentioned previously, the magnitude of the three-dimensional effects on the pressures in the separated region ahead of

finite-span ramps depend primarily on the span of the ramp and not significantly on the ramp chord if reattachment of the boundary layer occurs on the surface of the ramp (which is the case for all tests of the present investigation). However, in the present paper, the span has been divided by the constant ramp chord in order to nondimensionalize the span. The resultant ratio b/c is, by definition, the aspect ratio. Consequently, the following discussion is stated in terms of the aspect ratio b/c; however, the active variable is in reality the ramp span rather than the aspect ratio as such.

## Experimental Results

Effect of ramp deflection angle.- The center-line pressure distributions shown in figure 5 and the schlieren photographs of figure 6 indicate that boundary-layer separation results with all ramp deflections of the present investigation. The pressure rise upstream of the ramp leading edge and the essentially constant pressure plateau are typical characteristics of a separated laminar boundary layer and they occur for all ramp deflections and aspect ratios. (See fig. 5.) However, the location $x_o$ at which the separation interaction begins, as well as the pressures in the separated region, is significantly affected by changing the ramp deflection angle while keeping the other geometric and flow parameters constant. As the deflection angle of the ramp is increased, the location of the start of the pressure rise due to the separation moves upstream and results in a decrease in the Reynolds number $R_{x,o}$ at the start of the interaction. As might be expected, inasmuch as Chapman (ref. 2) indicates that the plateau pressure is inversely proportional to $R_{x,o}$, the plateau pressure also increases with ramp deflection angle. (See figs. 5 and 7.)

The location of the separation point was determined from schlieren photographs such as those shown in figure 6. The flow was assumed to separate from the surface of the flat plate directly below the intersection of the outer edge of the boundary layer and the shock wave generated by the separation region. (See figs. 1 and 6.) The variation

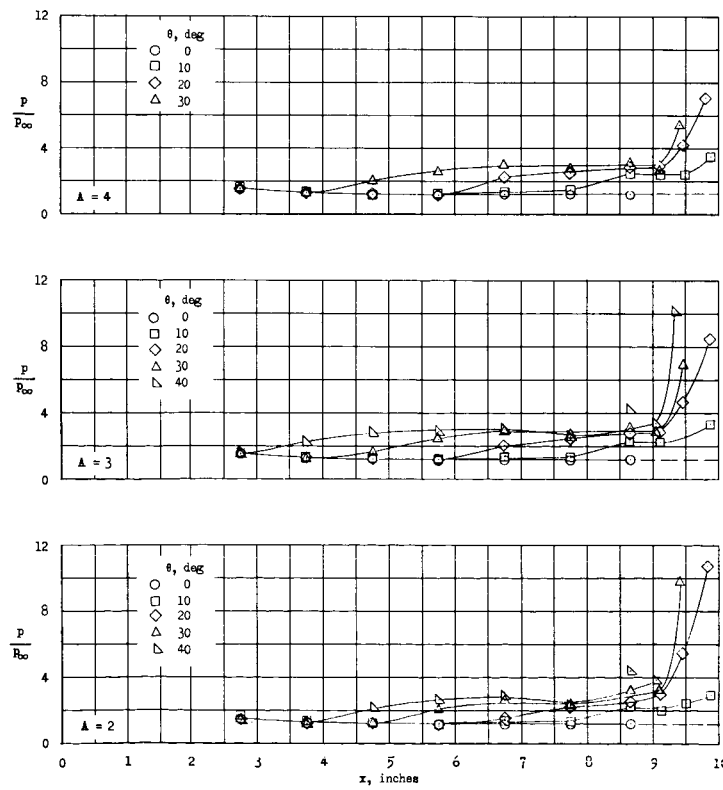


Figure 5.- Effect of ramp deflection angle on longitudinal pressure distribution on noninsulated flat plate. $y = 0$; $\frac{R}{x} \approx 1.27 \times 10^5$ per inch.

of the separation length (i.e., distance from separation point to ramp leading edge) with the ramp deflection angle for the ramps of various aspect ratios is shown in figure 7. The separation length appears to increase almost linearly with increasing ramp deflection angle within the range of the present data. This correlation of the separation length with ramp deflection angle agrees with references 3 and 17, which indicate that the separation length is proportional to the final pressure reached on the ramp (i.e., the pressure that would be reached on an infinitely long ramp). The ramp pressure, of course, increases with an increase in ramp angle. Figure 7 also shows a large effect of ramp aspect ratio on the length of separation.

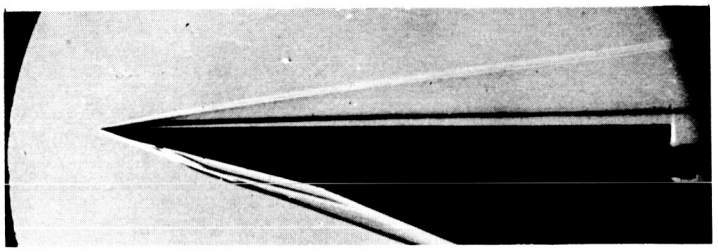

(a) $\theta = 0^{\circ}$.

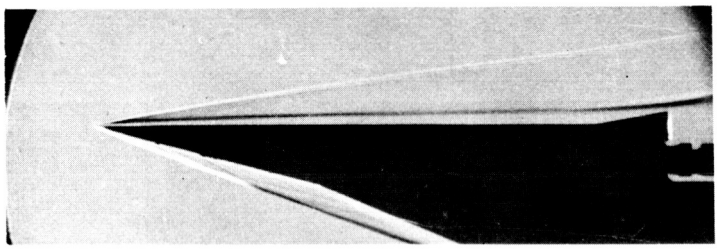

(b) $\theta = 10^{\circ}$; $A = 4$.

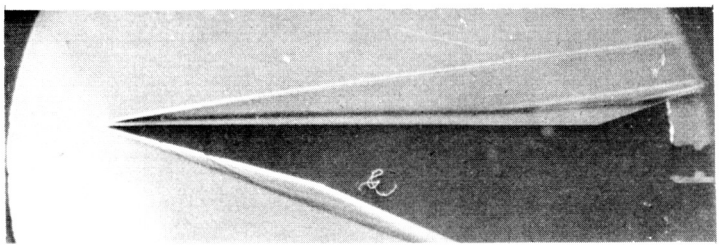

(c) $\theta = 20^{\circ}$; $A = 4$.

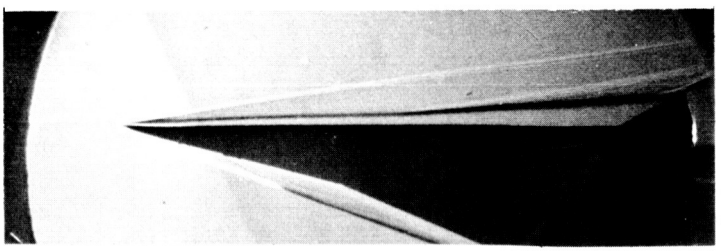

(d) $\theta = 30^{\circ}$; $A = 4$. L-65-37

Figure 6.- Typical schlieren photographs showing effects of ramp deflection angle. $\frac{R}{x} \approx 1.26 \times 10^{5}$ per inch.

Effects of ramp aspect ratio.- The effects of ramp aspect ratio on the three-dimensional pressure distribution on the flat plate are shown in figures 8 to 11. These figures show large effects of ramp aspect ratio on the extent of the separation region resulting from deflecting the ramps and also show large effects on the pressure distribution in the separated region. Decreasing the ramp aspect ratio from 4 to 2 results in decreases in the magnitude of the separation-induced pressures. Also, the location of the start of the separation pressure rise moves downstream on the flat plate with decreasing aspect ratio, and a corresponding increase in $R_{x,o}$ results. Two-dimensional separation theory, of course, does not explain the decrease in the length of the separation region with decreasing ramp aspect ratio; however, the theory does predict the decrease in the magnitude of the induced pressure rise to the constant plateau

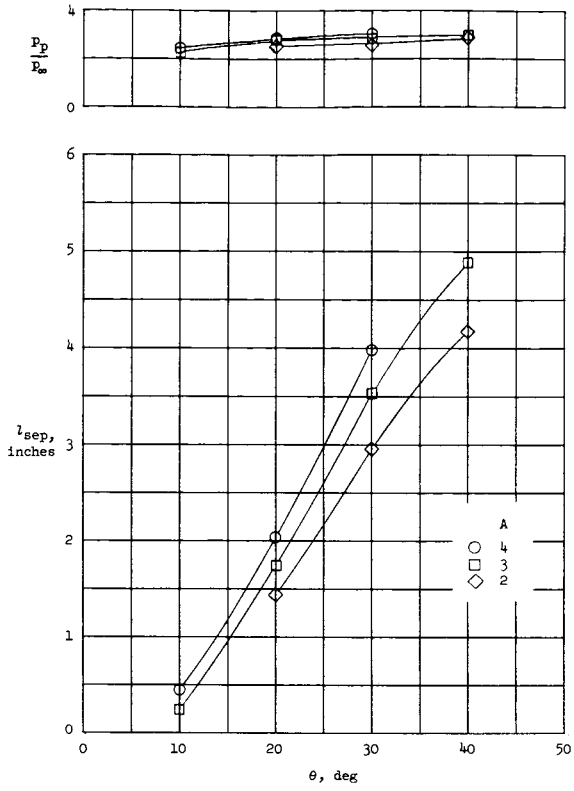


Figure 7.- Effect of ramp deflection angle on separation length and on plateau pressure. y = 0; $\frac{R}{x} \approx 1.26 \times 10^5$ per inch.

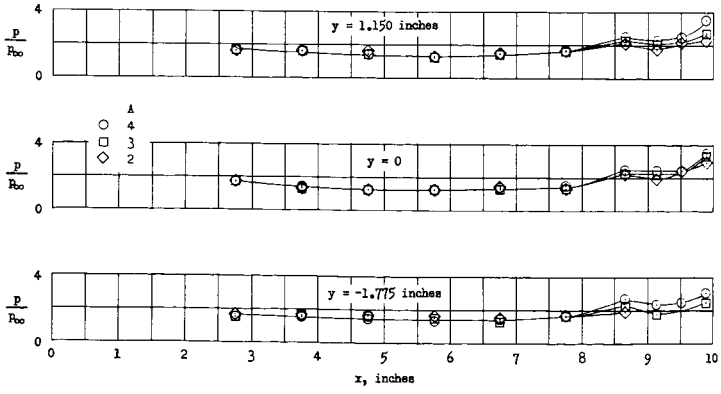


(a) Longitudinal pressure distribution.

Figure 8.- Effect of ramp aspect ratio on pressure distribution on noninsulated flat plate. θ = 10°; $\frac{R}{x} \approx 1.23 \times 10^5$ per inch.

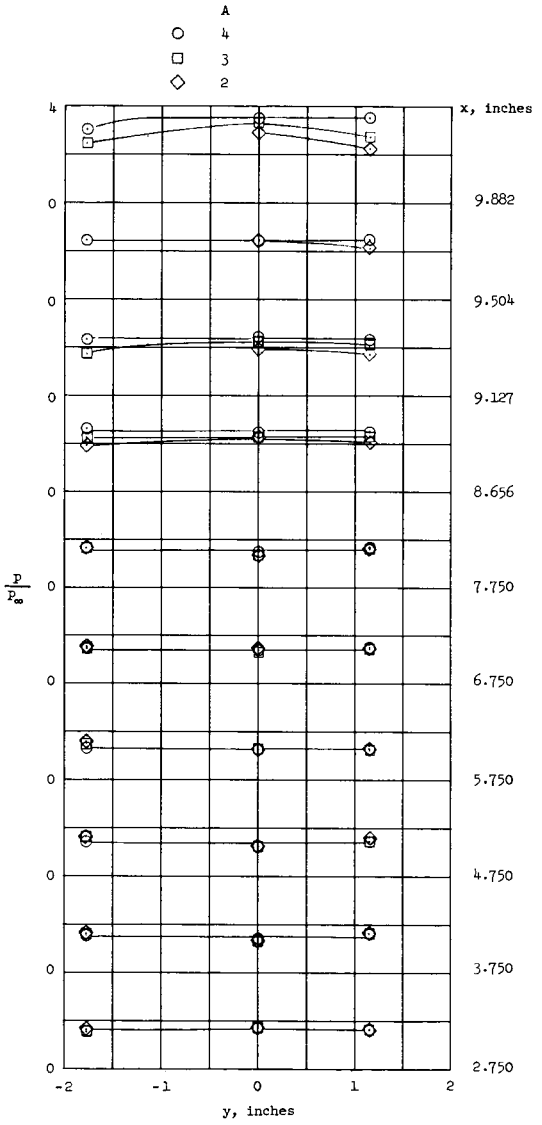


(b) Lateral pressure distribution.

Figure 8.- Concluded.

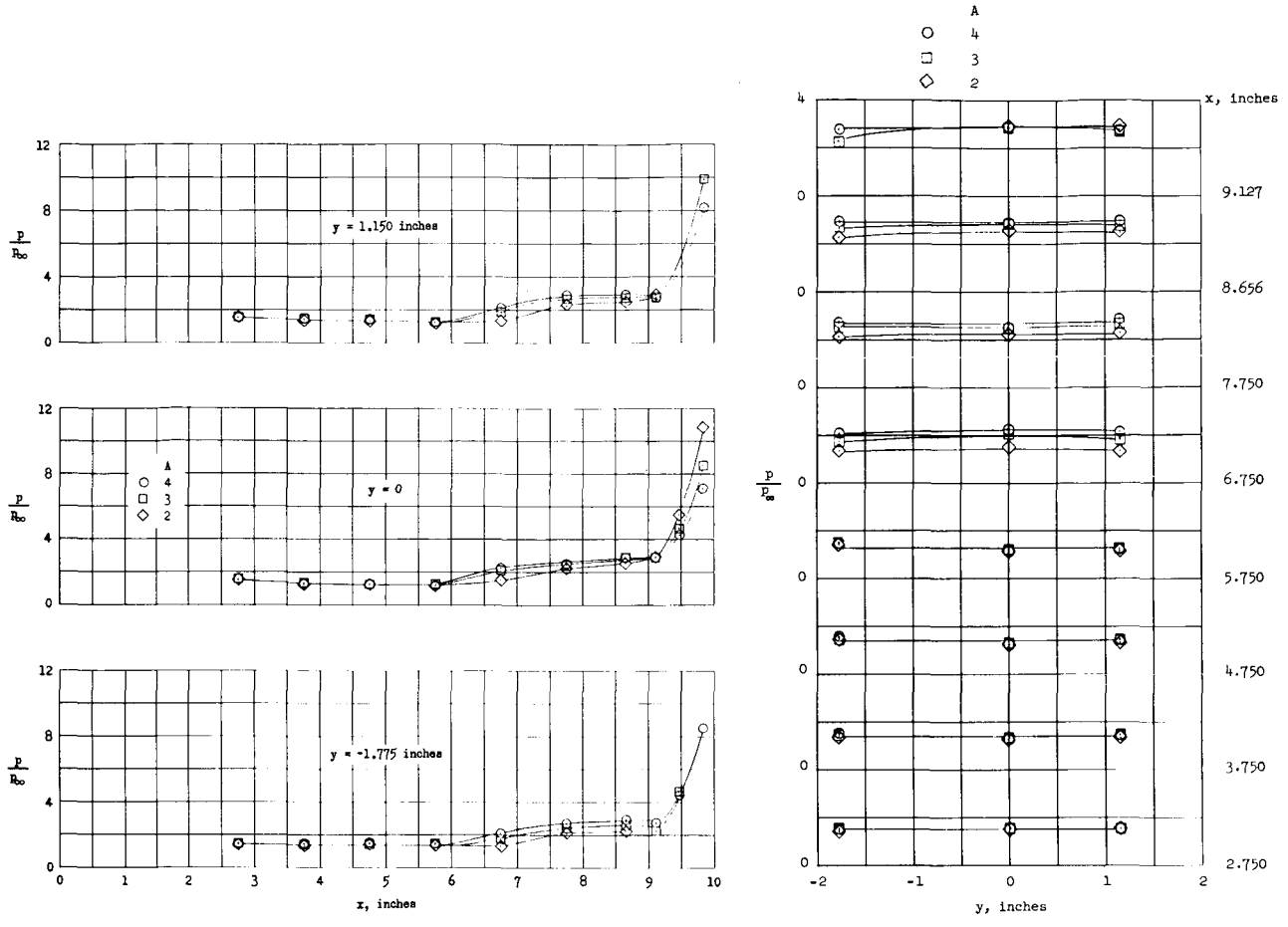


(a) Longitudinal pressure distribution. (b) Lateral pressure distribution.

Figure 9.- Effect of ramp aspect ratio on pressure distribution on noninsulated flat plate. $\theta = 20^{\circ}$; $\frac{R}{x} \approx 1.27 \times 10^{5}$ per inch.

pressure with the increase in $R_{x,o}$ resulting from the decrease in $l_{sep}$. The decrease in the length of the separation region is a three-dimensional effect, but the pressures in the three-dimensional separation region are influenced by the Reynolds number at the beginning of the interaction and therefore by the distance $x_o$ in the same manner as for two-dimensional flow separation. The lateral pressure distributions shown in figures 8(b), 9(b), 10(b), and 11(b) are essentially two-dimensional ($p/p_\infty$ constant with y) in the instrumented portion of the flat plate except in the area near the ramp leading edge. (It should be noted that the lateral pressure distributions in figures 8 to 11 are faired to agree with the fairings of the longitudinal pressure distributions.) In the area near the ramp edge (that is, near $x = 8.656$ in.), as can be seen from both the lateral and the longitudinal pressure distributions, the pressure decreases near the lateral edge of the ramp as a result of the outflow of the low-momentum air from the relatively high-pressure separated region at the ramp center to the low-pressure region outboard of the ramp edge. This outflow of the low-momentum air can be seen in the photographs and sketches of the oil-flow

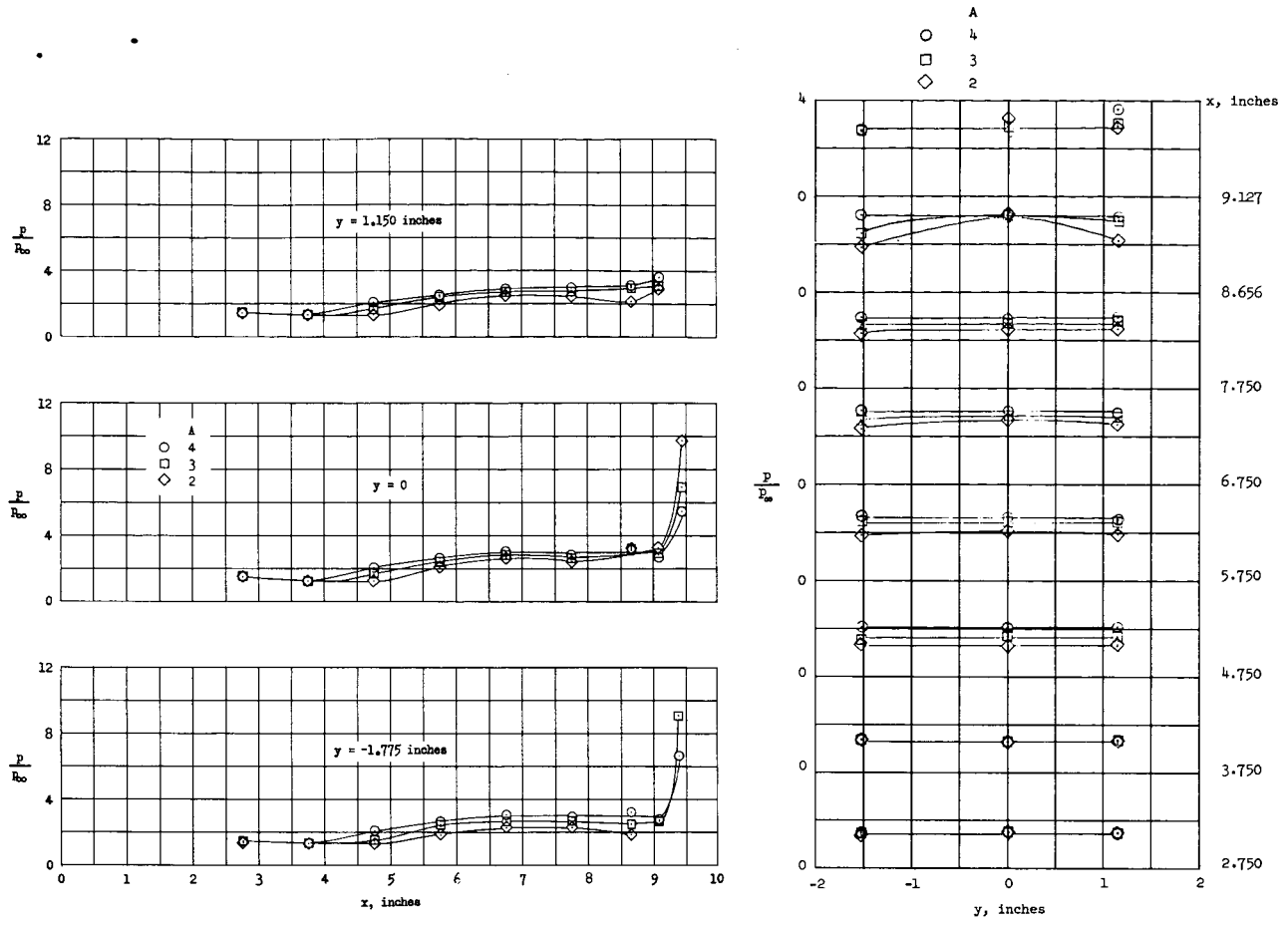


(a) Longitudinal pressure distribution. (b) Lateral pressure distribution.

Figure 10.- Effect of ramp aspect ratio on pressure distribution on noninsulated flat plate. $\theta = 30^{\circ}$; $\frac{R}{x} \approx 1.28 \times 10^{5}$ per inch.

patterns shown in figure 12. As a result of the outflow, there is probably a collapse of the overall displacement bubble, which lowers the "effective body" near the ramp edge and hence lowers the induced pressures. As the ramp deflection angle is increased this bleedout effect becomes more pronounced and results in appreciable reductions in the pressure near the outboard edge of the ramp. The effect of the bleedout of the low-momentum air has an increasingly important effect on the pressures in the separated region as the aspect ratio decreases. This effect can be seen from the three-dimensional plot in figure 13 of the pressure distribution on the flat plate with the ramp of A = 2 deflected 30°. The partial collapse of the region of vortex-type flow with decreasing aspect ratio and the corresponding decreases in pressures result in a decrease in the length of the separated region, inasmuch as the pressures in the separated region are functions of the distance to the separation-induced pressure rise. Therefore, there is a tendency for the three-dimensional separated flow to adjust itself so that the characteristic pressures in the separated region and $R_{x,o}$ (based on distance to interaction) satisfy equation (2).

As can be seen from the schlieren photographs of figure 14 and the curves of figure 15, the length of separation on the model center line varies almost

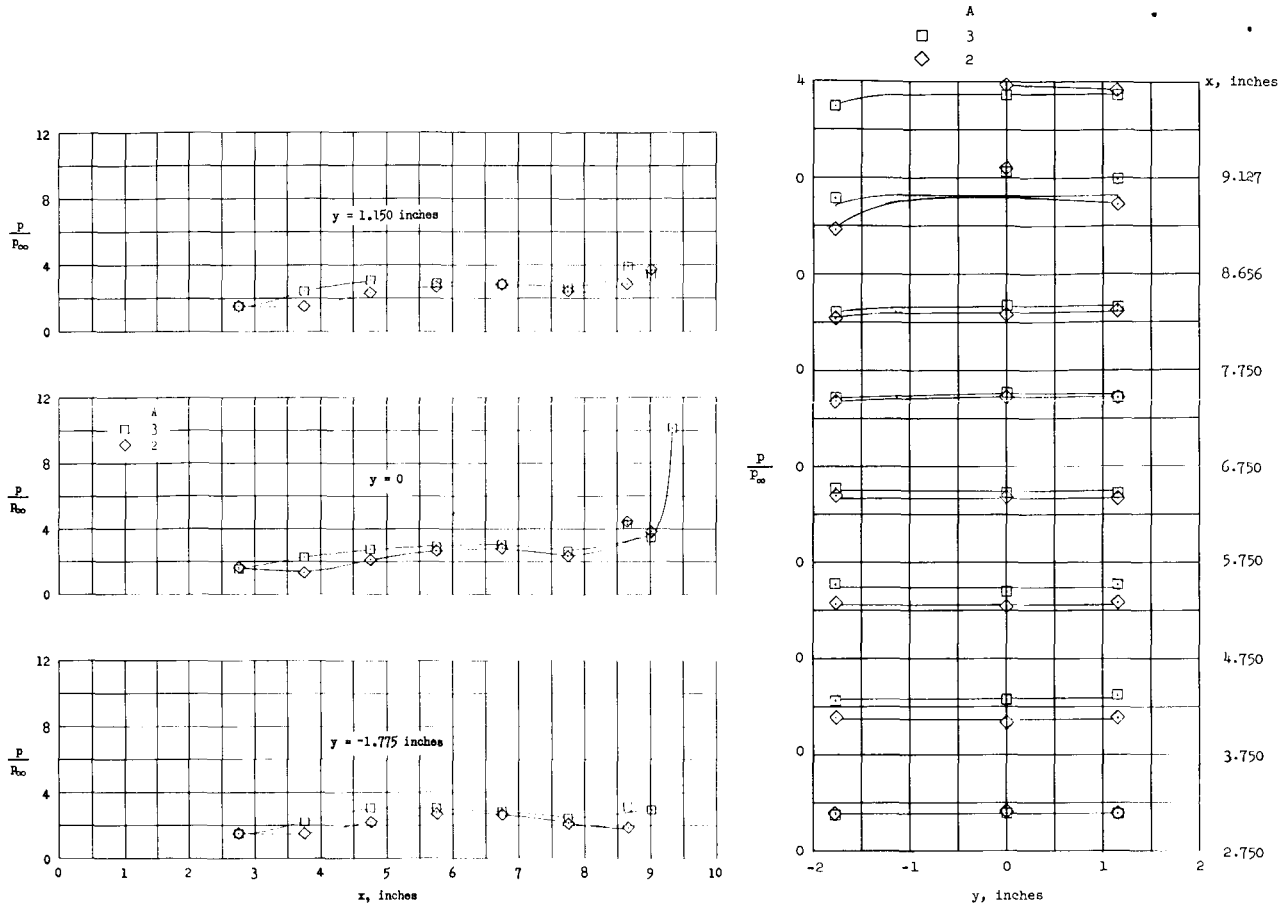


(a) Longitudinal pressure distribution. (b) Lateral pressure distribution.

Figure 11.- Effect of ramp aspect ratio on pressure distribution on noninsulated flat plate. $\theta = 40^{\circ}$; $\frac{R}{x} \approx 1.31 \times 10^{5}$ per inch.

linearly with the aspect ratio at a given ramp deflection angle. However, the variation of separation length with aspect ratio becomes more pronounced as the ramp angle is increased. A study of the pressure distributions in figures 8 to 11 indicates that there are only small differences in the magnitudes of $x_o$ at $y = 1.150$ inches, $y = -1.775$ inches, and at the model center line. Therefore, at least in the instrumented portion of the flat plate, there are only small three-dimensional effects on the length of separation. However, as can be seen from the oil-flow photographs in figure 12, the separation region extends outboard of the lateral edge of the ramps to the edge of the flat plate with a considerable lateral variation in the distance to the separation point $x_s$. The pressure distributions for the ramps of $A = 2$ at $y = -1.775$ inches, which is 0.525 inch outboard of the lateral edge of the ramp (figs. 8 to 11 and 13) indicate that the induced pressure rise also extends laterally a considerable distance outboard of the extremities of the ramp. Inasmuch as the separation length decreases with decreasing aspect ratio, the length of the separated laminar boundary layer resulting from inlets or the deflection of flap-type controls on hypersonic aircraft would probably be smaller than that which would be predicted by two-dimensional separation theory. However, the actual extent of the three-dimensional separated region may be considerably

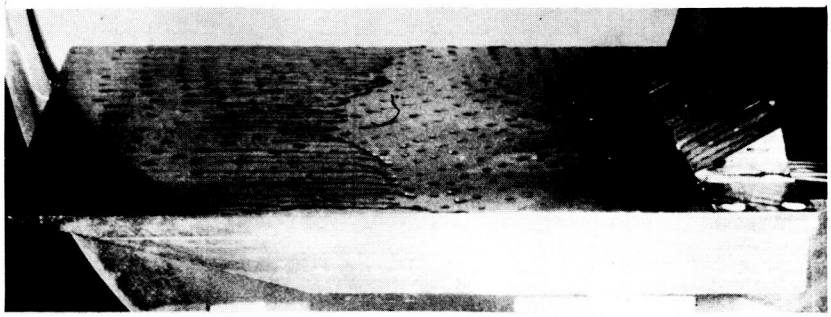

$\theta = 30^{\circ}$, A = 4.

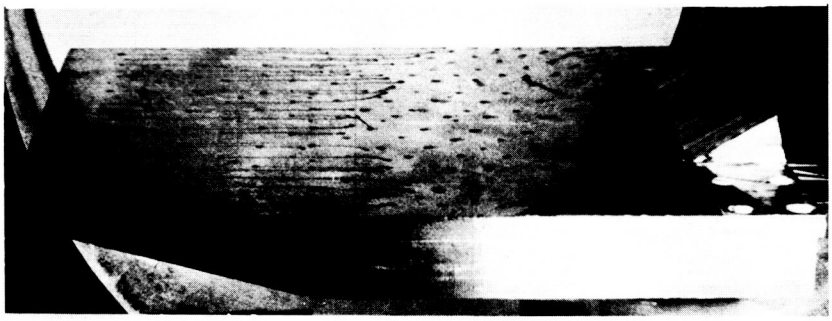

$\theta = 30^{\circ}$, A = 3.

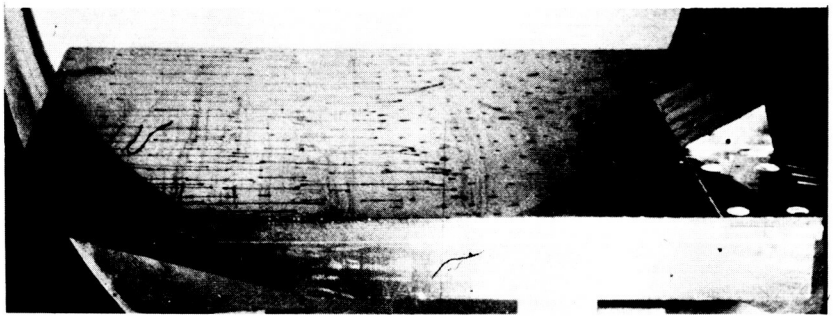

$\theta = 30^{\circ}$, A = 2.

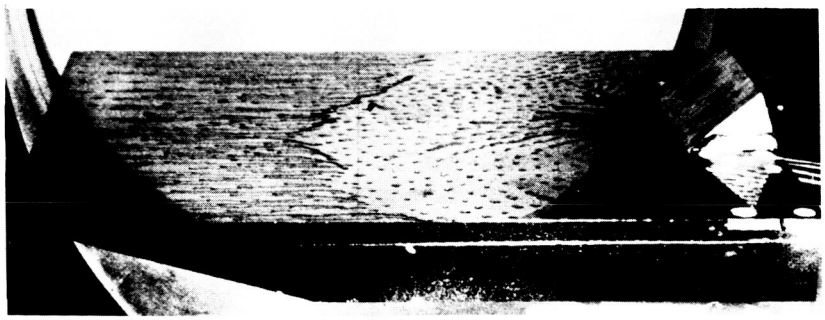

$\theta = 40^{\circ}$, A = 2.

(a) Photographs of oil-flow patterns. L-65-38

Figure 12.- Photographs and sketches of typical oil-flow patterns on flat plate with ramps of various deflection angles and aspect ratios.

greater than that predicted by two-dimensional separation theory because this region extends outboard of the lateral extremities of the flaps or inlets.

Effects of free-stream Reynolds number.- The effects of varying the free-stream Reynolds number from approximately $1.26 \times 10^5$ to $1.56 \times 10^5$ per inch on the pressure distribution on the flat plate are shown in figure 16. This Reynolds number variation had essentially no effect on the pressure distributions on the basic flat plate ($\theta = 0^\circ$) and on the ramp configurations with $\theta = 20^\circ$, $A = 4$, and $\theta = 40^\circ$, $A = 2$.

## Comparison of Experimental Results With Two-Dimensional Theory

Correlation of plateau pressure with $R_{x,o}$ and $M_o$.- The equations that have been developed for two-dimensional laminar boundary-layer separation provide a method of correlating the plateau pressures in a separated region with Mach number and Reynolds number. These equations (eqs. (2) and (3)) indicate that the plateau-pressure data should correlate if $C_{p,p}\beta_o^{1/2}$ is plotted as a function of $R_{x,o}$ or if $C_{p,p}R_{x,o}^{1/4}$ is plotted as a function of $M_o$. In order to evaluate these correlating functions, the Mach number, the Reynolds number, the wall temperature, and the static pressure at the start of the separation-induced pressure rise must be determined. A study of the separated pressure distributions in figure 5 indicates that the pressure first begins to rise approximately

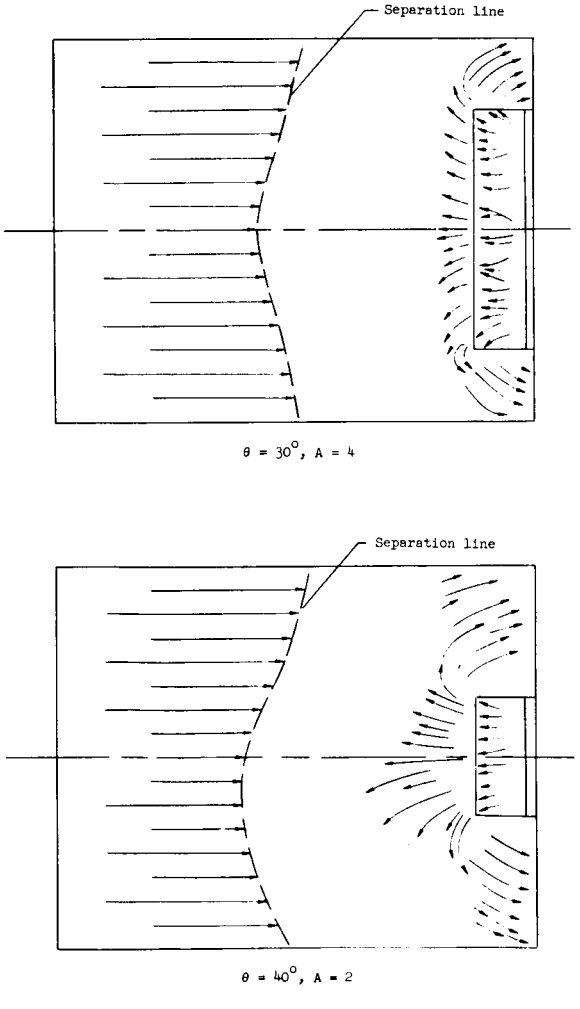


(b) Sketches of oil-flow patterns.

Figure 12.- Concluded.

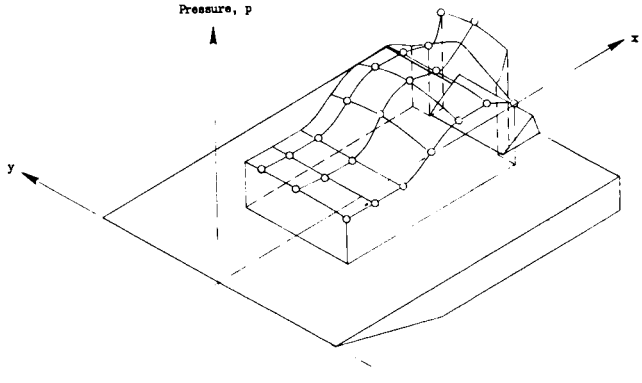


Figure 13.- Three-dimensional plot showing pressure distribution on flat plate. $\theta = 30^\circ$; $A = 2$; $\frac{R}{x} \approx 1.29 \times 10^5$ per inch.

1 inch ahead of the separation point. Therefore, $x_o$ has been assumed to be 1 inch ahead of the separation point ($x_o = x_s - 1$ in.) in the determination of $p_o$, $M_o$, and $R_{x,o}$. In the present investigation, the wall temperature and the static pressure at $x_o$ have been obtained by experiment. An estimation of the Mach number at $x_o$ may be obtained by assuming that it is equal to the Mach number of the flow over a two-dimensional wedge whose half-angle is such that the pressure on the surface of the wedge is equal to the experimental value of $p_o$; that is, $M_o$ can be determined from (ref. 28)

$$M_o = \left\{ \frac{M_\infty^2\left[(\gamma + 1)\xi + (\gamma - 1)\right] - 2(\xi^2 - 1)}{\xi\left[(\gamma - 1)\xi + (\gamma + 1)\right]} \right\}^{1/2}$$

where $\xi = \frac{p_o}{p_\infty}$. The Reynolds number $R_{x,o}$ at the beginning of the separation-induced pressure rise may be determined from the local Mach number, the stagnation temperature, the static pressure at $x_o$, and the distance $x_o$.

A correlation of the plateau-pressure data of the present investigation with Reynolds number is shown in figure 17(a) where $C_{p,p}\beta_o^{1/2}$ is plotted as a function of $R_{x,o}$. In this figure, the experimental data of the present investigation are compared with the correlation curve (eq. (2)) from reference 2, which is for flow over an insulated flat plate, and with the correlation curve (eq. (3)) from reference 17, which considers the effect of heat transfer. Generally, the experimental data tend to lie between the two-dimensional theoretical curves of references 2 and 17, and the experimental values of $C_{p,p}\beta_o^{1/2}$ decrease with increasing $R_{x,o}$ as predicted. The agreement between the two-dimensional separation theories and the experimental three-dimensional data indicates that the plateau pressures in a three-dimensional separated region depend on the same variables as the plateau pressures in a two-dimensional separation region.

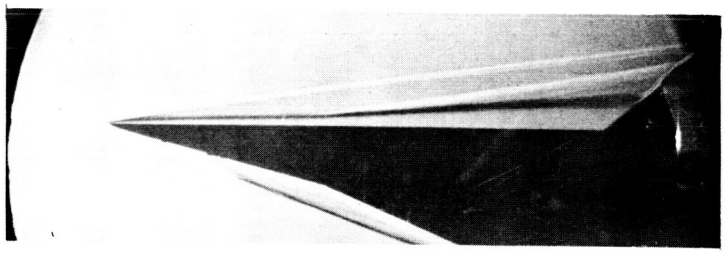

(a) $\theta = 40^\circ$; A = 3.

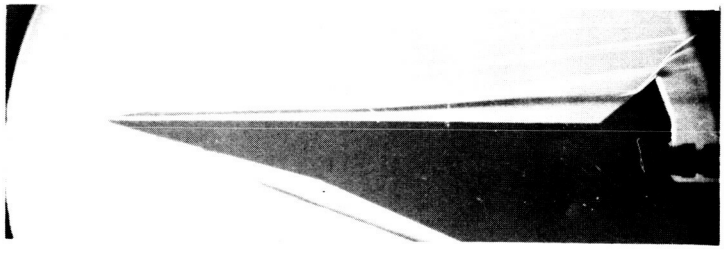

(b) $\theta = 40^\circ$; A = 2. L-65-39

Figure 14.- Typical schlieren photographs showing effects of ramp aspect ratio. $\frac{R}{x} \approx 1.31 \times 10^5$ per inch.

The plateau-pressure data of the present investigation (i.e., $M_\infty = 10.03$) are correlated with Mach number in figure 17(b) where $C_{p,p}R_{x,o}^{1/4}$ is plotted as a function of $M_o$. Also shown in this figure are two-dimensional plateau-pressure data obtained from references 2, 3, 19, and 26 for boundary-layer separation for values of $M_o$ from 1.3 to 16. The deviation of the present three-dimensional data with heat transfer from the two-dimensional theories of references 2 and 17 for flow over an insulated plate is of the same order of magnitude as the deviation of the two-dimensional data from the same theories at other Mach numbers.

Length of separation.- References 3 and 17 have suggested that the length of a two-dimensional laminar separation region is a function of the pressure rise from the constant-pressure plateau to the final pressure on the ramp. In order to determine whether the lengths of the three-dimensional separation region of the present investigation are functions of the same variables as the lengths of a two-dimensional separation region, the present data have been plotted in figure 18 as functions of the parameters suggested in references 3 and 17. Reference 3 suggests that the length of a two-dimensional separation region is a function of $\left(C_{p,f} - 1.21C_{p,p}\right)R_{x,o}^{-1/8}$. (See eq. (5).) The experimental data of the present investigation, however, do not include the final pressures on the ramps; therefore, $p_f$ has been determined by inviscid shock theory. As can be seen in figure 18(a), the separation lengths on the model center line are a function of the parameter suggested in reference 3 for a given ramp aspect ratio. Thus the length of a three-dimensional separation region appears to be a function of the same variables as the length of a two-dimensional separation region. However, the length of a three-dimensional separation region is, in addition, a function of ramp aspect ratio. At a given value of $\left(C_{p,f} - 1.21C_{p,p}\right)R_{x,o}^{-1/8}$, the length of separation decreases with decreasing aspect ratio.

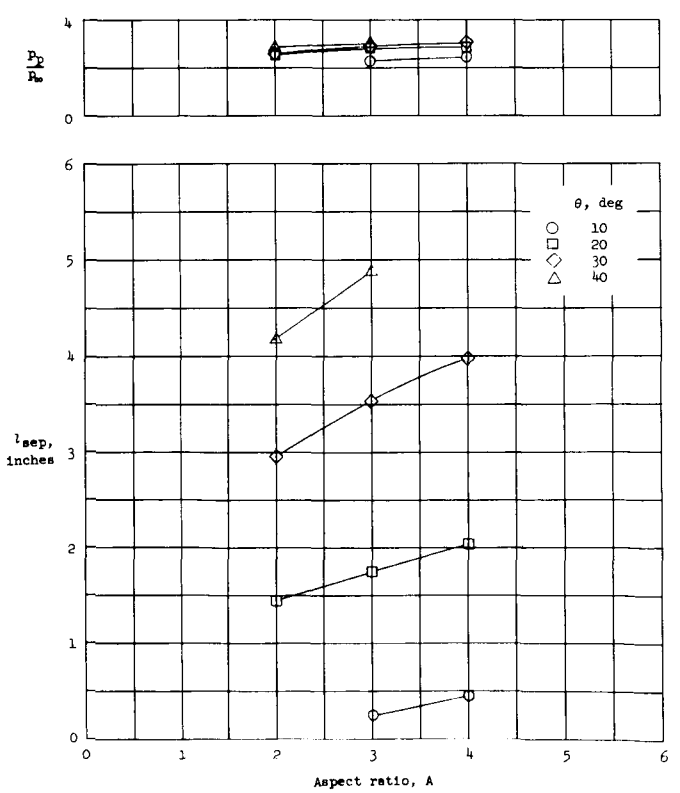


Figure 15.- Effect of ramp aspect ratio on separation length and plateau pressure. $y = 0$; $\frac{R}{x} \approx 1.26 \times 10^5$ per inch.

Reference 17 suggests that the length of a two-dimensional

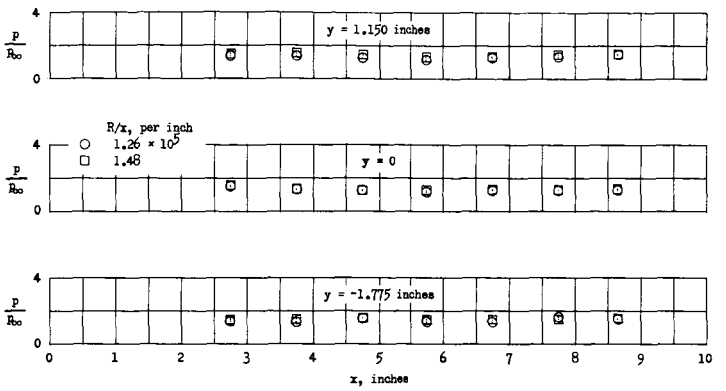


(a) $\theta = 0^{\circ}$.

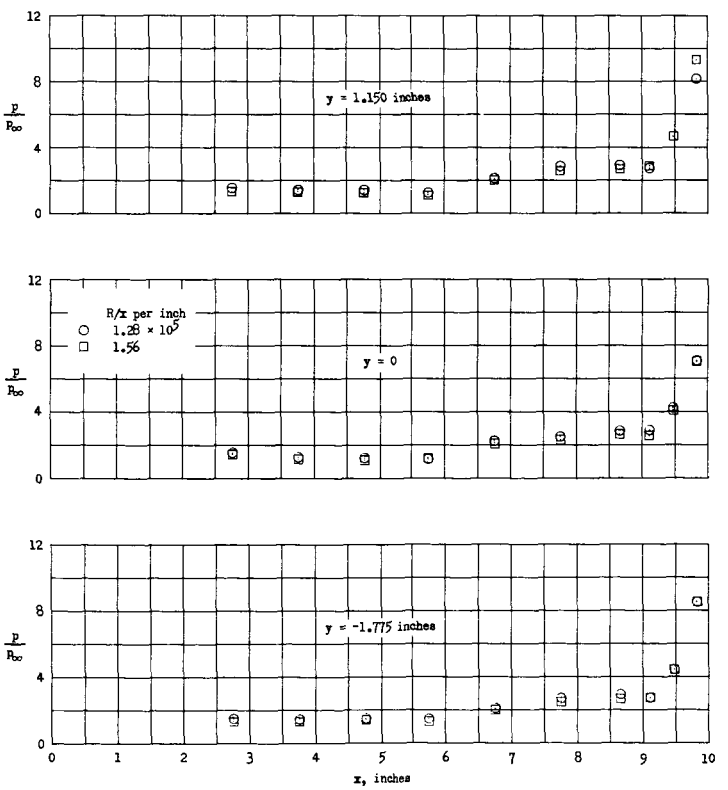


(b) $\theta = 20^{\circ}$; A = 4.

Figure 16.- Effect of Reynolds number on pressure distribution on noninsulated flat plate with ramps of various deflection angles and aspect ratios.

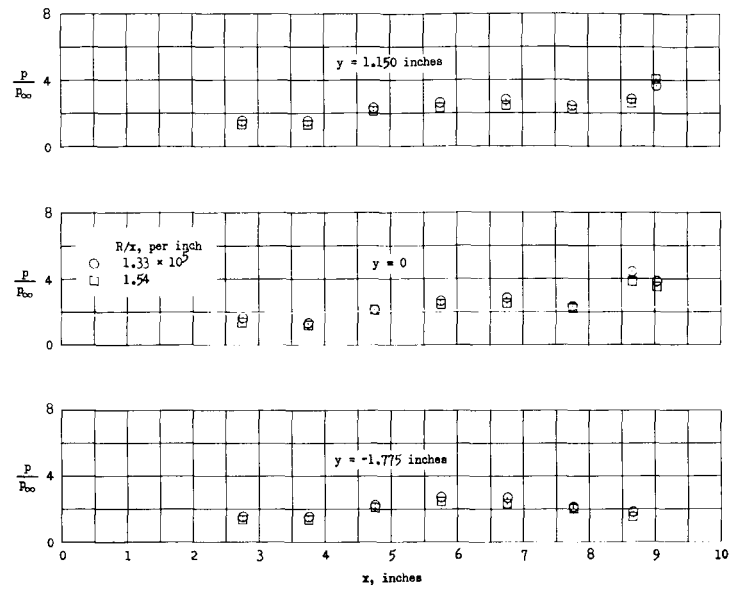


(c) $\theta = 40^\circ$; A = 2.

Figure 16.- Concluded.

separation region is a function of $\frac{p_f - p_p}{p_o}$. (See eq. (6).) The separation lengths on the model center line for the present investigation are plotted as a function of $\frac{p_f - p_p}{p_o}$ in figure 18(b). The final pressures on the ramps for figure 18(b) were also determined by inviscid shock theory. The nondimensional separation length $\frac{l_{sep}}{\delta_o}$ ($\delta_o$ determined experimentally from schlieren photographs) is an almost linear function of the final pressure-rise coefficient $\frac{p_f - p_p}{p_o}$ at a given ramp aspect ratio. As can be seen from figure 18(b), at a given value of $\frac{p_f - p_p}{p_o}$, the nondimensional separation length decreases with decreasing aspect ratio.

These results (fig. 18) indicate that the length of a separation region resulting from a finite-span ramp is a function of the same parameters (i.e., $p_f$, $p_p$, and $p_o$) as the length of a separated region in two-dimensional flow. In addition, the three-dimensional separation length is also a function of ramp aspect ratio. The separation length is probably also a function of the Mach number, the free-stream Reynolds number, and possibly the wall temperature on the flat plate; however, there was no attempt to evaluate the effect of these parameters on the length of separation in the present investigation.

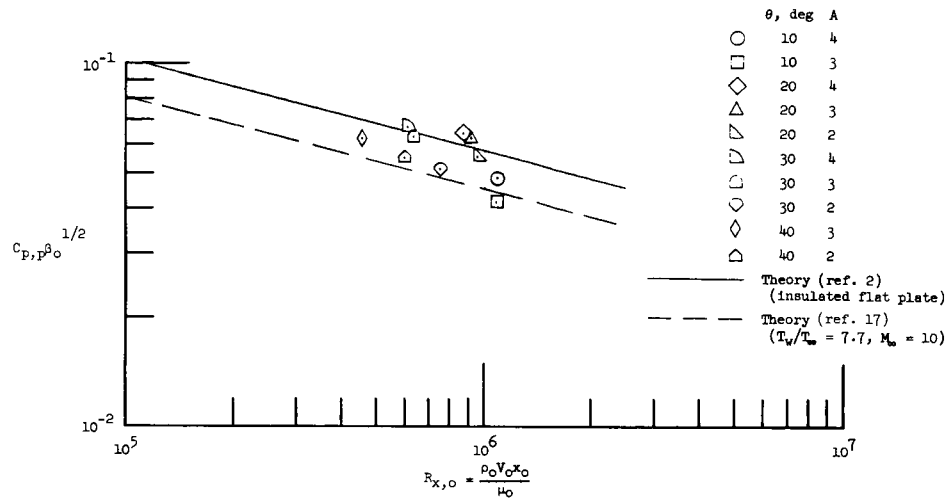


(a) Correlation of $C_{p,p}\beta_o^{1/2}$ with $R_{x,o}$. ($p_o$ determined experimentally.)

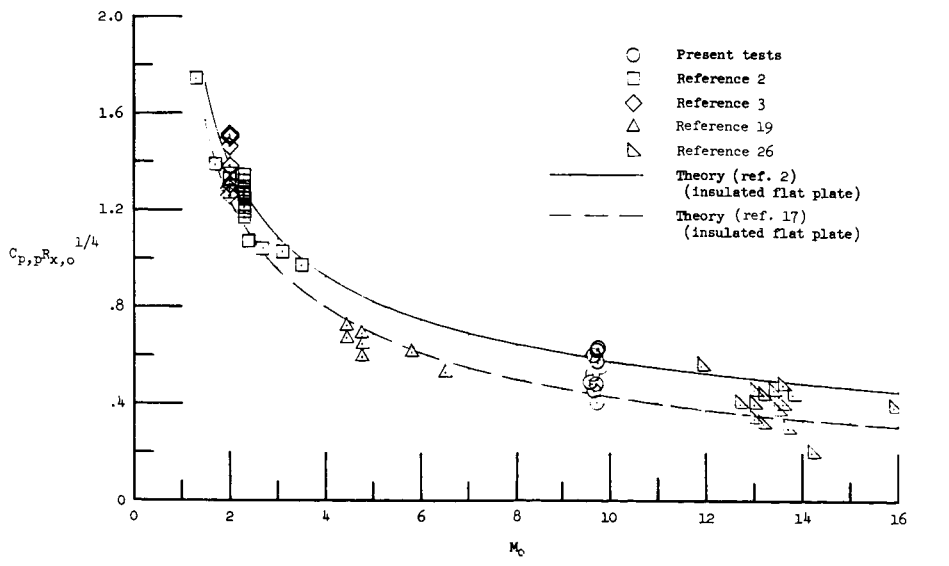


(b) Correlation of $C_{p,p}R_{x,o}^{1/4}$ with $M_o$.

Figure 17.- Correlation of plateau pressure with Reynolds number and Mach number.

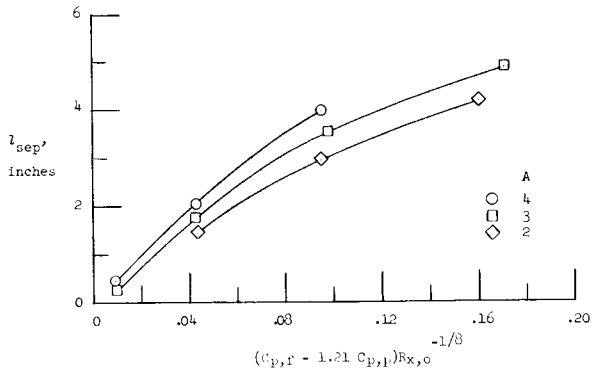


(a) Variation of $l_{sep}$ with $\left(C_{p,f} - 1.21C_{p,p}\right)R_{x,o}^{-1/8}$.

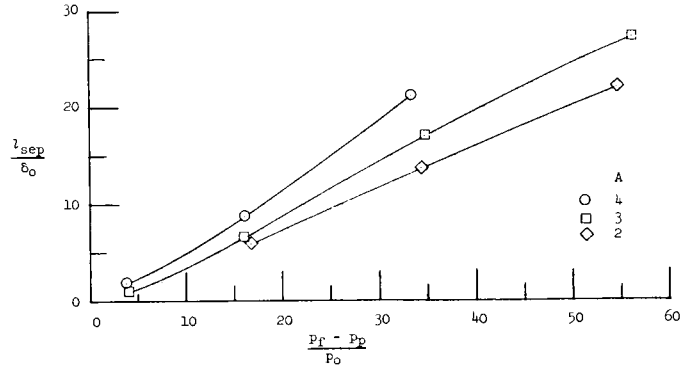


(b) Variation of $\frac{l_{sep}}{\delta_o}$ with $\frac{p_f - p_p}{p_o}$.

Figure 18.- Variation of length of separation with various functions of final pressure-rise coefficient. ($p_f$ computed by inviscid theory.) y = 0.

## CONCLUDING REMARKS

An investigation has been made of the effects of ramp deflection angle and ramp span on laminar boundary-layer separation at a free-stream Mach number of 10.03. The study was undertaken to establish the extent and magnitude of the separation-induced pressure distribution on flat surfaces ahead of small-span ramps and to evaluate the usefulness of two-dimensional theoretical methods for correlating and predicting the characteristics of three-dimensional separation.

The experimental results indicate that increasing the deflection angle of a finite-span ramp on a flat plate from $10^{\circ}$ to $40^{\circ}$ resulted in an increase in the length of the region of separated flow along the model center line and an increase in the magnitude of the pressures in the separation region. Decreasing the ramp aspect ratio (i.e., the ramp span) from 4 to 2 at a given deflection angle results in a rearward movement of the separation point and a decrease in magnitude of the pressures in the separated region. The results show that the length of separation along the model center line decreases almost linearly with decreasing aspect ratio for constant ramp angles; however, the separation length is more strongly influenced by aspect ratio as the ramp deflection angle is increased. Data for the ramps of aspect ratio 2 and oil-flow observations indicate that the separation-induced pressure rise extends a considerable distance outboard of the lateral edge of the three-dimensional (i.e., finite span) ramps.

Methods suggested by two-dimensional separation theory generally result in a good correlation of the plateau pressure-rise coefficients obtained on the center line of the flat plate with Reynolds number and Mach number. The results also show that the length of a three-dimensional separation region is a function of the same parameters as the length of a two-dimensional separation region, but in addition, the length of a three-dimensional separation region also depends on the ramp aspect ratio (i.e., the ramp span). Therefore, these effects of ramp aspect ratio must be considered when predicting the characteristics of a separated laminar boundary layer ahead of a finite-span ramp.

Langley Research Center,
National Aeronautics and Space Administration,
Langley Station, Hampton, Va., February 18, 1965.

# APPENDIX

## AIR CONDENSATION

Air condensation occurs in a hypersonic nozzle when the decreasing pressure and temperature of the expanding flow reach or exceed the air saturation point (i.e., the combination of pressure and temperature for which a component of air first condenses). To avoid condensation, the air in the tunnel must be heated to stagnation temperatures sufficiently high so that the static air temperatures throughout the expansion are greater than the saturation temperature. For tunnels operating at a hypersonic Mach number, however, this approach becomes difficult because of the very high stagnation temperatures required.

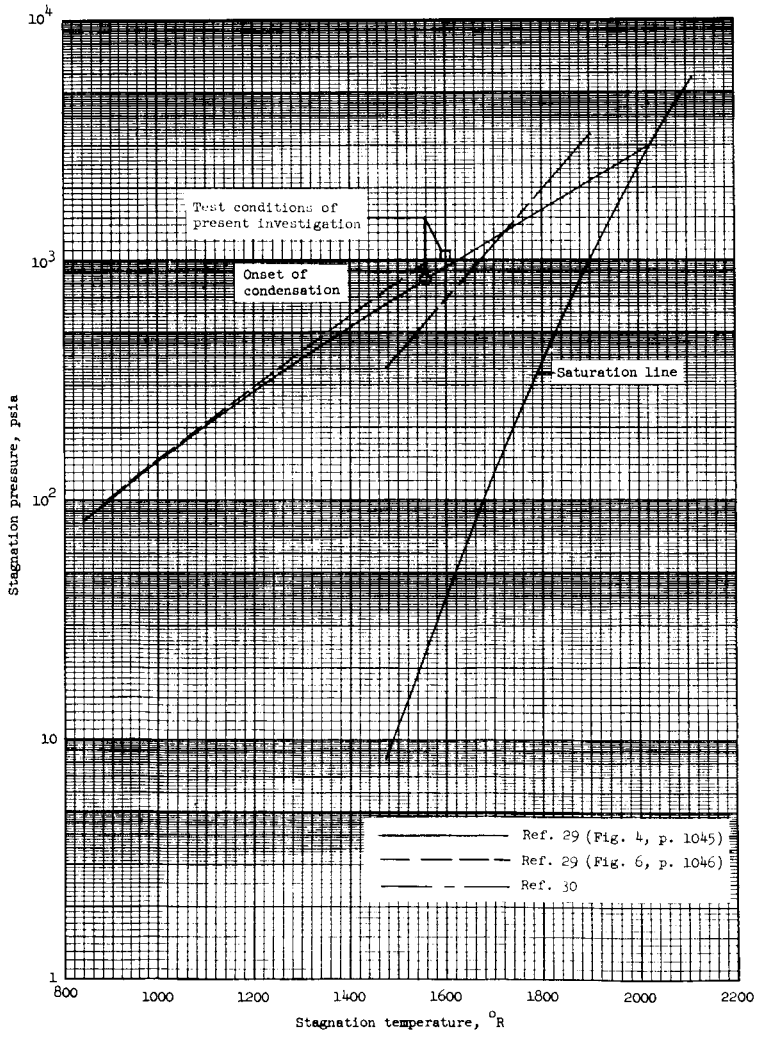


Figure A-1.- Stagnation temperature and pressure at onset of air condensation. M = 10.03.

The present tests were conducted at stagnation temperatures below those theoretically required for avoiding air saturation in order to extend the operating life of the direct-current resistance tube heater used in the Langley 15-inch hypersonic flow apparatus. The stagnation temperatures used in the present tests (on the order of 1100° F) were selected on the basis of a detailed study of available experimental data on condensation effects (for example, refs. 29 and 30) which indicated that, as a result of supersaturation of the expanding flow, stagnation temperatures well below those theoretically required are sufficient to prevent air condensation in a wind tunnel. This decrease in the required stagnation temperature resulting from the effects of supersaturation (i.e., a condition in which the air expands to a temperature lower than the saturation temperature without the onset of condensation) can best be seen in figure A-1. This figure shows the theoretical

values of stagnation temperature and pressure for which the air expanding in a nozzle to a Mach number of 10.03 would become saturated and also shows the values of stagnation temperature and pressure at which air condensation actually occurs. The curves for the onset of condensation were taken from the experimental data of references 29 and 30. These results indicate that, for the stagnation pressures of the present tests, a stagnation temperature approximately 300° F below the temperature required to prevent air saturation can be used without the occurrence of condensation.

In figure A-2 the effects of stagnation temperature on the pressure distributions on the noninsulated flat plate at M = 10.03 are shown. As can be seen in this figure, a variation in stagnation temperature from 1032° F to 1208° F and from 1163° F to 1205° F at free-stream unit Reynolds numbers of approximately $1.37 \times 10^5$ and $1.44 \times 10^5$ per inch, respectively, had essentially no effect on the pressure distributions on the flat plate. In order to determine the stagnation temperature at which air condensation begins significantly to affect data obtained in the Langley 15-inch hypersonic flow apparatus, tests have been made at constant stagnation pressure with varying stagnation temperature. The results of these experiments are shown in figures A-3 and A-4. At a stagnation pressure of 825 psia, significant effects of air condensation on the tunnel wall static pressure and the tunnel pitot pressure do not occur until the stagnation temperature has been reduced below about 950° F. (See fig. A-3.) The effect of stagnation temperature on the

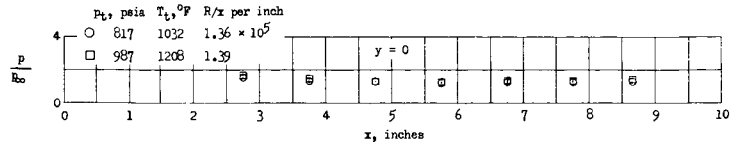


(a) $\frac{R}{x} \approx 1.37 \times 10^5$ per inch.

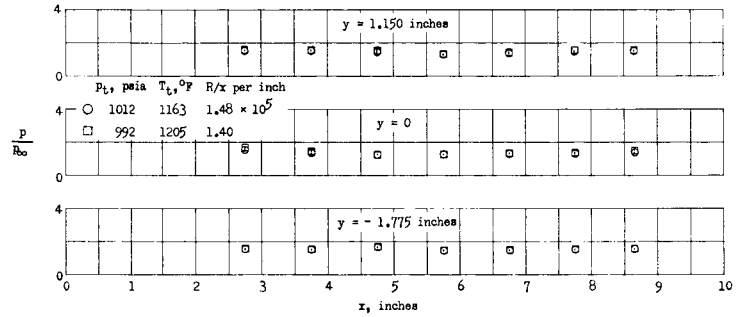


(b) $\frac{R}{x} \approx 1.44 \times 10^5$ per inch.

Figure A-2.- Effect of stagnation temperature on pressure distribution on noninsulated flat plate.

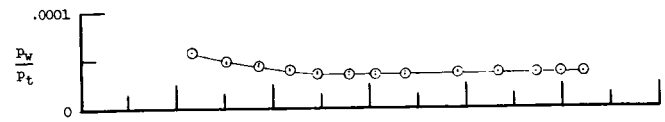


(a) Variation of tunnel-wall static pressure with $T_t$.

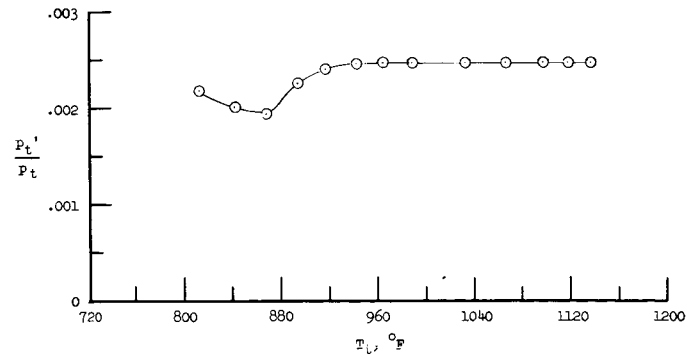


(b) Variation of pitot pressure with $T_t$.

Figure A-3.- Effect of stagnation temperature on tunnel-wall static pressure and pitot pressure in Langley 15-inch hypersonic flow apparatus at $p_t$ = 825 psia.

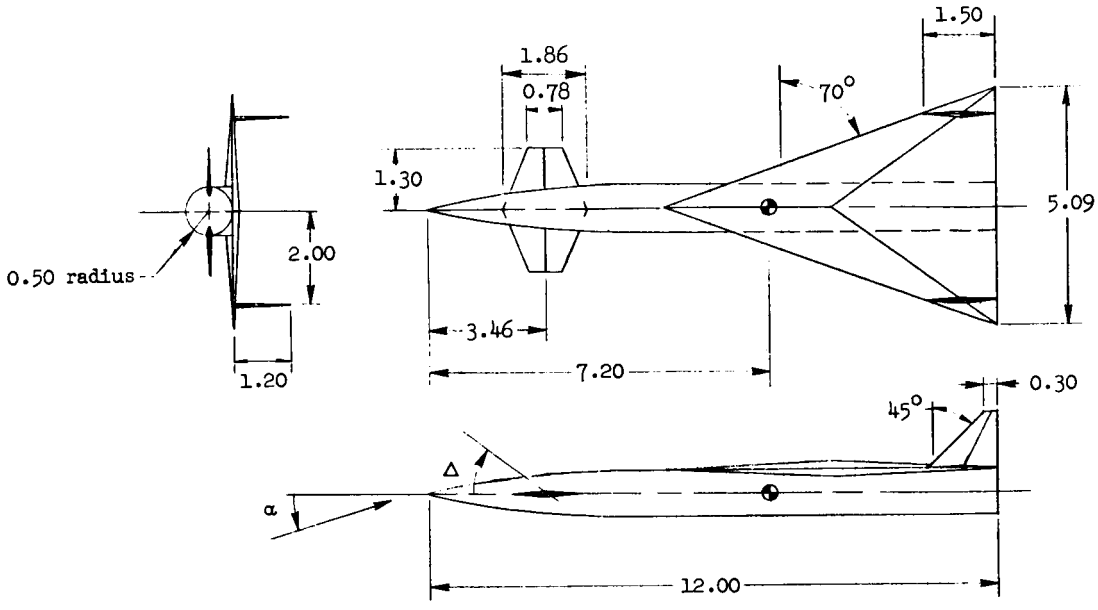


(a) Sketch of model. (All dimensions are in inches unless otherwise noted.)

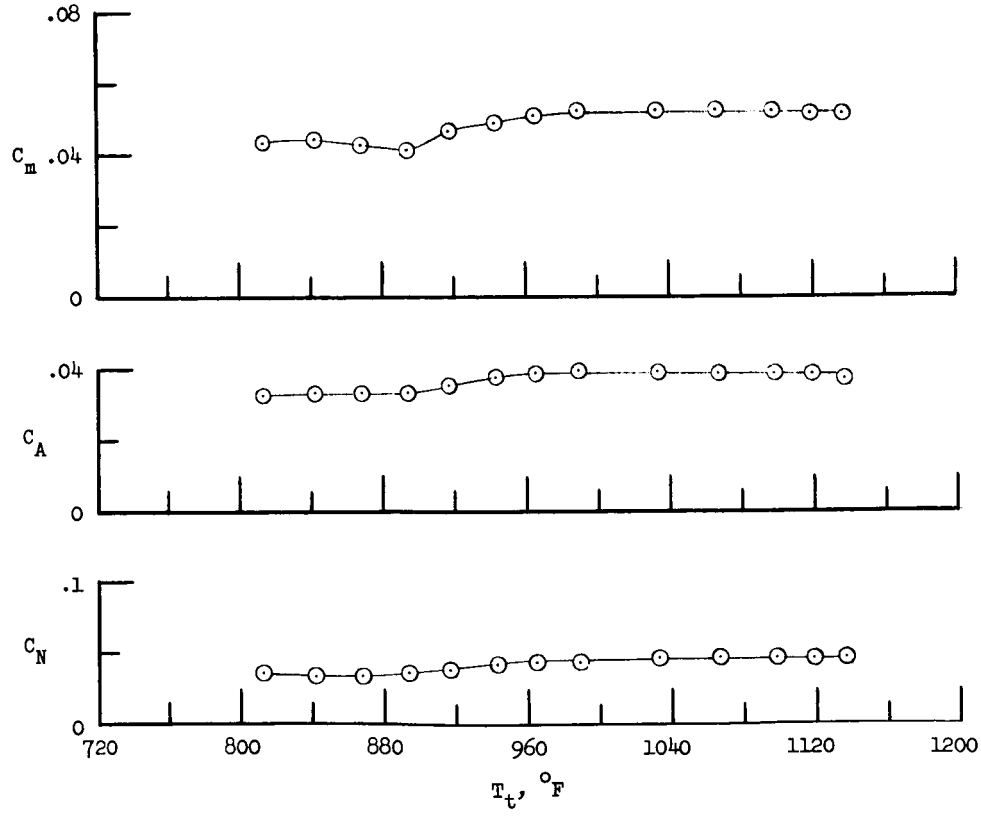


(b) Variation of $C_N$, $C_A$, and $C_m$ with $T_t$ for $\alpha = 0.1^\circ$ and $\Delta = 20^\circ$.

Figure A-4.- Effect of stagnation temperature on force and moment characteristics of a typical hypersonic model in Langley 15-inch hypersonic flow apparatus at $p_t$ = 825 psia.

force and moment data for a typical hypersonic airplane model is shown in figure A-4. These results show that at $p_t$ = 825 psia, air condensation effects on force and moment data are not important at temperatures greater than about 970° F. These experimental results obtained in the Langley 15-inch hypersonic flow apparatus indicate that stagnation temperatures in the vicinity of 1100° F (as in the present tests) are sufficient to prevent air condensation in the tunnel at stagnation pressures in the vicinity of 825 psia.

## REFERENCES


1. Potter, J. Leith; and Whitfield, Jack D.: Effects of Unit Reynolds Number, Nose Bluntness, and Roughness on Boundary Layer Transition. AEDC-TR-60-5 (Contract No. AF 40(600)-800), Arnold Eng. Dev. Center, Mar. 1960.

2. Chapman, Dean R.; Kuehn, Donald M.; and Larson, Howard K.: Investigation of Separated Flows in Supersonic and Subsonic Streams With Emphasis on the Effect of Transition. NACA Rept. 1356, 1958. (Supersedes NACA TN 3869.)

3. Hakkinen, R. J.; Greber, I.; Trilling, L.; and Abarbanel, S. S.: The Interaction of an Oblique Shock Wave With a Laminar Boundary Layer. NASA MEMO 2-18-59W, 1959.

4. Gadd, G. E.: A Theoretical Investigation of Laminar Separation in Supersonic Flow. J. Aeron. Sci., vol. 24, no. 10, Oct. 1957, pp. 759-771.

5. Gadd, G. E.: A Thoeretical Investigation of the Effects of Mach Number, Reynolds Number, Wall Temperature and Surface Curvature on Laminar Separation in Supersonic Flow. Rept. No. F.M. 2415, Brit. A.R.C., June 13, 1956.

6. Gadd, G. E.; Holder, D. W.; and Regan, J. D.: An Experimental Investigation of the Interaction Between Shock Waves and Boundary Layers. Proc. Roy. Soc. (London), ser. A, vol. 226, no. 1165, Nov. 9, 1954, pp. 227-253.

7. Greber, Isaac: Interaction of Oblique Shock Waves With Laminar Boundary Layers. Tech. Rept. 59-2, M.I.T., Apr. 28, 1959.

8. Amick, James L.: A Semiempirical Relation for Laminar Separation. J. Aero/Space Sci. (Readers' Forum), vol. 26, no. 9, Sept. 1959, pp. 603-604.

9. Gadd, G. E.; and Holder, D. W.: The Behaviour of Supersonic Boundary Layers in the Presence of Shock Waves. Paper No. 59-138, Inst. Aeron. Sci., Oct. 1959.

10. Guman, William J.: On the Plateau and Peak Pressure of Regions of Pure Laminar and Fully Turbulent Separation in Two-Dimensional Supersonic Flow. J. Aero/Space Sci., vol. 26, no. 1, Jan. 1959, p. 56.

11. Greber, Isaac: Shock-Wave Laminar-Boundary-Layer Interaction on a Convex Wall. NASA TN D-512, 1960.

12. Le Blanc, L. P.; and Webb, H. G., Jr.: Boundary Layer Separation in a Supersonic Stream. Rept. No. SID 61-72, North Am. Aviation, Inc., Mar. 1961.

13. Sanders, F.; and Crabtree, L. F.: A Preliminary Study of Large Regions of Separated Flow in a Compression Corner. Tech. Note No. Aero. 2751, Brit. R.A.E., Mar. 1961.

14. Brower, W. B., Jr.: Leading-Edge Separation of Laminar Boundary Layers in Supersonic Flow. J. Aerospace Sci., vol. 28, no. 12, Dec. 1961, pp. 957-961.

15. Curle, N.: Heat Transfer and Laminar-Boundary-Layer Separation in Steady Compressible Flow Past a Wall with Non-Uniform Temperature. R. & M. No. 3179, Brit. A.R.C., 1961.

16. Glick, Herbert S.: Modified Crocco-Lees Mixing Theory for Supersonic Separated and Reattaching Flows. J. Aerospace Sci., vol. 29, no. 10, Oct. 1962, pp. 1238-1249.

17. Erdos, John; and Pallone, Adrian: Shock-Boundary Layer Interaction and Flow Separation. RAD-TR-61-23, Res. and Advanced Develop. Div., AVCO Corp., Aug. 15, 1961.

18. Kaufman, Louis G., II; Hartofilis, Stavros A.; Evans, William J.; Oman, Richard A.; Meckler, Lawrence H.; and Weiss, Daniel: A Review of Hypersonic Flow Separation and Control Characteristics. ASD TDR 62-168, U.S. Air Force, 1962.

19. Sterrett, James R.; and Emery, James C.: Extension of Boundary-Layer-Separation Criteria to a Mach Number of 6.5 by Utilizing Flat Plates With Forward-Facing Steps. NASA TN D-618, 1960.

20. Sterrett, James R.; and Emery, James C.: Experimental Separation Studies for Two-Dimensional Wedges and Curved Surfaces at Mach Numbers of 4.8 to 6.2. NASA TN D-1014, 1962.

21. Graham, W. J.; and Vas, I. E.: An Experimental Investigation of the Separation of a Hypersonic Boundary Layer of a Flat Plate - Part I: Pressure Distribution and Optical Studies at M = 11.7. ARL 63-74, U.S. Air Force, May 1963.

22. Bogdonoff, S. M.; and Vas, I. E.: Some Experiments on Hypersonic Separated Flows. ARS J., vol. 32, no. 10, Oct. 1962, pp. 1564-1572.

23. Abbott, Douglas E.; Holt, Maurice; and Nielsen, Jack N.: Studies of Separated Laminar Boundary Layers at Hypersonic Speed With Some Low Reynolds Number Data. [Preprint] No. 63-172, Am. Inst. Aeron. Astronaut., June 1963.

24. Michel, Roger: Conditions de décollement de la couche limite laminaire a grande altitude aux vitesses hypersoniques. La Rech. Aeron. (O.N.E.R.A.), no. 91, Nov.-Dec. 1962, pp. 3-12.

25. Nielsen, Jack N.; and Goodwin, Frederick K.: Investigation of Hypersonic Flow Separation and Its Effect on Aerodynamic Control Characteristics. Rept. No. 63 (Contract No. AF 33(657)-7084), Vidya, Inc., Jan. 1962.

26. Miller, D. S.; Hijman, R.; and Childs, M. E.: Mach 8 to 22 Studies of Flow Separations Due to Deflected Control Surfaces. AIAA J., vol. 2, no. 2, Feb. 1964, pp. 312-321.

27. Putnam, Lawrence E.; and Brooks, Cuyler W., Jr.: Static Longitudinal Aerodynamic Characteristics at a Mach Number of 10.03 of Low-Aspect-Ratio Wing-Body Configurations Suitable for Reentry. NASA TM X-733, 1962.

28. Ames Research Staff: Equations, Tables, and Charts for Compressible Flow. NACA Rept. 1135, 1953. (Supersedes NACA TN 1428.)

29. Daum, Fred L.: Air Condensation in a Hypersonic Wind Tunnel. AIAA Jour., vol. 1, no. 5, May 1963, pp. 1043-1046.

30. Goranson, George G.; Jaffe, Peter; Steuer, Guenter; and Dayman, Bain, Jr.: Additional Observations of the Effects of Air Condensation in the 21-Inch Hypersonic Wind Tunnel. Tech. Release No. 34-153 (Contract NASw-6), Jet Propulsion Lab., C.I.T., Oct. 26, 1960.



NASA-Langley, 1965 L-4208